HORIZONTAL REASSIGNMENT SYNCHROSQUEEZING TRANSFORM FOR TIME-FREQUENCY ANALYSIS OF SEISMIC DATA

WEI LIU[1,2], SHUYAO ZHANG[1,2], KAIFANG CHEN[1,2] and SHUANGXI LI[1,2]

[1] *College of Mechanical and Electrical Engineering, Beijing University of Chemical Technology, North Third Ring Ring 15, Chaoyang District, Beijing 100029, P.R. China. liuwei_upc@126.com*
[2] *Beijing Key Laboratory of Health Monitoring Control and Fault Self-Recovery for High-End Machinery, Beijing University of Chemical Technology, North Third Ring 15, Chaoyang District, Beijing 100029, P.R. China. lishuangxi@mail.buct.edu.cn*

ABSTRACT

Liu, W., Zhang, S.Y., Chen, K.F. and Li, S.X., 2022. Horizontal reassignment synchrosqueezing transform for time-frequency analysis of seismic data. *Journal of Seismic Exploration*, 31: 325-339.

The short-time Fourier transform (STFT)-based synchrosqueezing transform (FSST) is a special type of reassignment method that achieves a compact time-frequency representation (TFR) for a class of nonstationary signal. However, for the signals with a strongly varying instantaneous frequency, the FSST method is always not desirable. To address the problem, a new method, termed as horizontal reassignment synchrosqueezing transform (HRSST), is proposed in the paper. By means of an unbiased group delay (GD) estimation, the HRSST provides a sharped TFR for transient signals in which the time-frequency ridge is nearly parallel with frequency axis. Through synthetic data, the proposed HRSST method is determined to be an effective and robust tool which provides superior results over some classical TFA techniques such as STFT and FSST. Finally, two field examples are employed to further demonstrate its potential in time localization characterization and subsurface geological structures delineation with high precision.

KEY WORDS: time-frequency representation, synchrosqueezing transform, horizontal reassignment synchrosqueezing transform, hydrocarbon detection, geological structures.

INTRODUCTION

Time-frequency analysis (TFA) always plays an important role in seismic data analysis (Castagna et al., 2003; Liu and Fomel, 2013; Chen et al., 2014; Liu and Chen, 2019; Liu and Duan, 2020). Over the past few decades, numerous TFA methods have been developed and widely applied in processing and interpretation of seismic data. The short-time Fourier transform (STFT) (Allen, 1977) and the continuous wavelet transform (CWT) (Sinha et al., 2005) are two commonly used TFR tools. The STFT implements Fourier transform with a sliding window to obtain a local time-frequency representation (TFR). However, such transform suffers from the Heisenberg uncertainty principle. Moreover, the STFT is sensitive to the selection of window function, that is, once the window is fixed, the time-frequency resolution is also determined. The CWT achieves a TFR with variable resolution with the help of a wavelet family. Unfortunately, the time and frequency resolutions cannot be simultaneously enhanced. Wigner-Ville distribution (WVD) (Jeffrey, 1999) makes a tradeoff between time and frequency resolutions, but the existence of cross-term interference limits time-frequency readability of seismic signal, and makes it challenging in real application.

In order to overcome above-mentioned problems, many efforts have been made to improve the time-frequency resolution. Auger and Flandrin (1995) introduced the reassignment method (RM) to sharp the TFR, in which it improves time-frequency energy concentration by transferring the time-frequency coefficients from the original position to the center of gravity of signal's energy distribution in both the time and frequency directions. Nevertheless, the RM faces with the disadvantage, namely, it does not allow for signal retrieval. Recently, the synchrosqueezing transform (SST) as a sparse representation is proposed by Daubechies et al. (2011), which is based on wavelet transform and has a solid theoretical foundation. Besides, the SST is also an adaptive and invertible tool that enhances the readability of TFR by condensing the spectrum along the frequency axis (Herrera et al., 2014). The SST was originally developed in the field of audio processing as a post-processing technique (Daubechies and Maes, 1996). Thakur and Wu (2011) further extended 'synchrosqueezing' idea to STFT and put forward the STFT-based SST (FSST). However, it is worth noting that both of the SST and FSST need meet the condition of weak frequency modulation hypothesis for the modes constituting the signal, which means that the two methods are unable to cope with the signals with strongly varying instantaneous frequency. To this end, Oberlin et al. (2015) attempted to establish the second-order synchrosqueezing transform (SST2) by a second-order local estimate of the instantaneous frequency. Afterwards, the SST2 was further generalized to the N-order version, called high-order synchrosqueezing transform, using higher order approximations both for the amplitude and phase (Pham and Meignen, 2017; Liu et al., 2020).

In this paper, we propose a novel TFA method, termed as horizontal

reassignment synchrosqueezing transform (HRSST), which aims at the signals with a strongly varying instantaneous frequency. First, a signal model in the frequency domain is defined. Then, the group delay (GD) related with frequency is utilized to extract the ridge. Finally, the reassignment operation is utilized in order to rearrange the coefficients of STFT in the horizontal direction.

This paper is structured as follows: in Section II, we recall some fundamental notation and definitions on STFT and FSST. Then, we present our technique, called horizontal reassignment synchrosqueezing transform (HRSST) in Section III. Section IV delivers numerical results on both synthetic signal and field data, and compares the proposed HRSST method with standard STFT and FSST, which further illustrates the potential of HRSST in geological structures delineation and hydrocarbon-saturated reservoir identification.

THEORETICAL BASIS

Short-time Fourier transform (STFT)

The Fourier transform of a given signal f is defined as follows:

$$\hat{f}(\varsigma) = \int_R f(t) e^{-i2\pi\varsigma t} dt \quad , \tag{1}$$

where t and ς are the time and frequency variables, respectively.

If $\hat{f}$ is integrable, f can be retrieved by:

$$f(t) = \int_R \hat{f}(\varsigma) e^{i2\pi\varsigma t} d\varsigma \quad . \tag{2}$$

It is well known that the Fourier transform $\hat{f}(\varsigma)$ describes the frequency information of signal f for the whole time, so that it is not suitable for depicting non-stationary signal where the frequency has the time localization. Thus, the short-time Fourier transform (STFT) was introduced, and the (modified) STFT of a given signal f is represented as:

$$V_f^g(t,\varsigma) = \int_R f(\tau) g^*(\tau - t) e^{-i2\pi\varsigma(\tau - t)} d\tau \quad , \tag{3}$$

where g is a window function, g^* denotes the complex conjugate of g, $\left| V_f^g(t,\varsigma) \right|^2$ is the spectrogram of signal f.

The original signal f can be reconstructed from its STFT using the following formula:

$$f(t) = \frac{1}{g^*(0)} \int_R V_f^g(t,\varsigma) d\varsigma \quad . \tag{4}$$

Note that g does not vanish and is continuous at 0.

STFT-Based SST (FSST)

Unlike RM, the key idea of FSST is to improve the time-frequency energy concentration by reassigning only the coefficients $V_f^g(t,\varsigma)$ according to the map $(t,\varsigma) \to \left(t, \hat{\omega}_f(t,\varsigma)\right)$.

The frequency operator $\hat{\omega}(t,\varsigma)$ that estimates the instantaneous frequency (IF) at time t and frequency ς is defined as:

$$\hat{\omega}_f(t,\varsigma) = \frac{1}{2\pi} \partial_t \arg\left[V_f^g(t,\varsigma)\right] = R\left[\frac{1}{i2\pi} \frac{\partial_t V_f^g(t,\varsigma)}{V_f^g(t,\varsigma)}\right] \quad , \tag{5}$$

where $R[\bullet]$ denotes the real part of a complex number, ∂_t represents the partial derivative with respect to time t.

Thus, the FSST is defined by:

$$T_f^g(t,\omega) = \frac{1}{g^*(0)} \int_{\{\varsigma, |V_f^g(t,\varsigma)| > \lambda\}} V_f^g(t,\varsigma) \delta\left(\omega - \hat{\omega}(t,\varsigma)\right) d\varsigma \quad , \tag{6}$$

where λ is some threshold, δ denotes the Dirac function, and ω denotes the frequency variable.

Finally, the mode $f_i(t)$ constituting the original signal f can be approximately recovered using the following formula:

$$f_i(t) \approx \int_{\{\omega, |\omega - \varphi_i(t)| < c\}} T_f^g(t,\omega) d\omega \quad , \tag{7}$$

where c is a compensation factor and $\varphi_i(t)$ is an estimate for IF.

HORIZONTAL REASSIGNMENT SYNCHROSQUEEZING TRANSFORM

It is noteworthy that the FSST is theoretically limited by the assumption of weak frequency modulation for the modes making up the signal. However, in real situation, most signals are composed of strong frequency modulated contents. Therefore, a new TFR method is required.

With regard to eq. (1), in the frequency domain, $\hat{f}(\varsigma)$ can be further defined by:

$$\hat{f}(\varsigma) = A(\varsigma)e^{i2\pi\psi(\varsigma)} \quad . \tag{8}$$

Then, the group delay (GD) can be written as:

$$\tau(\varsigma) = -\frac{d\psi(\varsigma)}{d\varsigma} \quad . \tag{9}$$

According to Parseval's theorem, the STFT in eq. (3) can be rewritten in the frequency domain as:

$$V_f^g(t,\varsigma) = V_f^G(t,\varsigma) = \frac{1}{2\pi}\int_R F(\xi)G^*(\xi-\varsigma)e^{-i2\pi t(\xi-\varsigma)}d\xi \quad , \tag{10}$$

where $F(\xi)$ and $G(\varsigma)$ denote the Fourier transforms of signal f and window function g, respectively.

One takes the partial derivative of $V_f^G(t,\varsigma)$ with respect to t and ς, then the following equations can be obtained.

$$\partial_\varsigma V_f^G(t,\varsigma) = -V_f^{G'}(t,\varsigma) - i2\pi t V_f^G(t,\varsigma) \quad , \tag{11}$$

$$\partial_t V_f^G(t,\varsigma) = i2\pi V_f^{\varsigma G}(t,\varsigma) \quad , \tag{12}$$

where $V_f^{G'}(t,\varsigma)$ and $V_f^{\varsigma G}(t,\varsigma)$ denote the STFTs of $F(\xi)$ with the windows G' and ςG, respectively.

Next, the reassignment operators $\tilde{v}_f(t,\varsigma)$ and $\tilde{\omega}_f(t,\varsigma)$ are respectively defined as ($V_f^G(t,\varsigma) \neq 0$):

$$\tilde{v}_f(t,\varsigma) = -\frac{\partial_\varsigma V_f^G(t,\varsigma)}{i2\pi V_f^G(t,\varsigma)} \quad , \tag{13}$$

$$\tilde{\omega}_f(t,\varsigma) = \varsigma + \frac{\partial_t V_f^G(t,\varsigma)}{i2\pi V_f^G(t,\varsigma)} \quad . \tag{14}$$

And, the second-order local modulation operator $\tilde{q}_f(t,\varsigma)$ is defined by:

$$\tilde{q}_f(t,\varsigma) = \frac{\partial_t \tilde{v}_f(t,\varsigma)}{\partial_t \tilde{\omega}_f(t,\varsigma)} \quad \text{when } \partial_t \tilde{\omega}_f(t,\varsigma) \neq 0 \qquad . \qquad (15)$$

Then, the second-order local GD estimate of signal f is defined as:

$$\tilde{v}_f^{[2]}(t,\varsigma) = \begin{cases} \tilde{v}_f(t,\varsigma) + \tilde{q}_f(t,\varsigma)\left(\varsigma - \tilde{\omega}_f(t,\varsigma)\right) & \text{if } \partial_t \tilde{\omega}_f \neq 0 \\[2mm] \tilde{v}_f(t,\varsigma) & \text{otherwise} \end{cases} \qquad (16)$$

where $\hat{v}_f^{[2]}(t,\varsigma) = R\left[\tilde{v}_f^{[2]}(t,\varsigma)\right]$ is the estimated GD.

Finally, the horizontal reassignment synchrosqueezing transform (HRSST) is expressed as:

$$T_{HRSST,f}^{G}(t,\varsigma) = \frac{1}{G^*(0)} \int_{\{t,|V_F^G|>\gamma\}} V_f^{G}(\mu,\varsigma)\delta\left(t - \hat{v}_f^{[2]}(\mu,\varsigma)\right)d\mu, \quad (17)$$

where γ is the threshold.

Furthermore, the inverse Fourier transform can be performed to retrieve the mode.

$$\hat{f}(t) = F^{-1}\left(\int_R T_{HRSST,f}^{G}(t,\varsigma)dt\right) \quad , \qquad (18)$$

where $F^{-1}(\bullet)$ denotes the inverse Fourier transform.

SYNTHETIC DATA

This section presents a synthetic signal, shown in Fig. 1, to illustrate the improvements brought by HRSST in comparison with the conventional STFT and FSST methods. The corresponding TFRs of the STFT, FSST, and HRSST are displayed in Fig. 2(a)-(c). It can be found that the TFR result from the STFT suffers from a poor time-frequency resolution due to the fixed window. Comparing with Fig. 2(a), one notices that the FSST provides a relatively nice TFR result. However, for the signals with a strongly varying instantaneous frequency, both STFT and FSST fail to give

a desired result. In contrast, the HRSST shows a clearly sharp TFR, especially in the time direction, which is more helpful for feature extraction of the strong frequency modulated signals. In order to clearly compare the performance of the aforementioned methods, we enlarged some areas indicated by the rectangles in Fig. 2, which are depicted in Fig. 3. One can clearly see the advantage of the HRSST in enhancing the energy concentration is highlighted in the time direction, which provides the potential in delineating thin-bed for seismic interpretation.

For a better understanding of the improvements brought by the use of HRSST, we will compare more quantitatively the three methods in terms of the sharpness of the representation. Herein, the Renyi entropy is utilized to evaluate the performances of the STFT, FSST and HRSST methods, and a lower Renyi entroy means a more energy-concentrated TFR. The corresponding Renyi entropy is listed in Table 1. It can be observed that the HRSST has the lowest Renyi entropy, that is, it can achieve the most energy-concentrated TFR. The Renyi entropy can be expressed as:

$$I = -\frac{1}{2}\log_2\left(\frac{\iint_{R^2}|T(t,\varsigma)|^3\,d\varsigma dt}{\iint_{R^2}|T(t,\varsigma)|\,d\varsigma dt}\right) \quad , \tag{19}$$

where $T(t,\varsigma)$ denotes the TFR result.
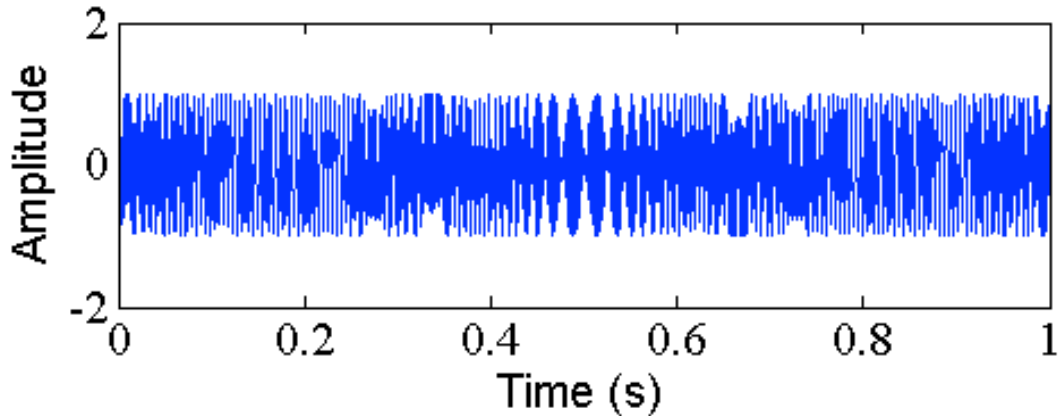
Fig.1. A synthetic signal.

Table 1. Renyi entropy of the STFT, FSST and HRSST methods.

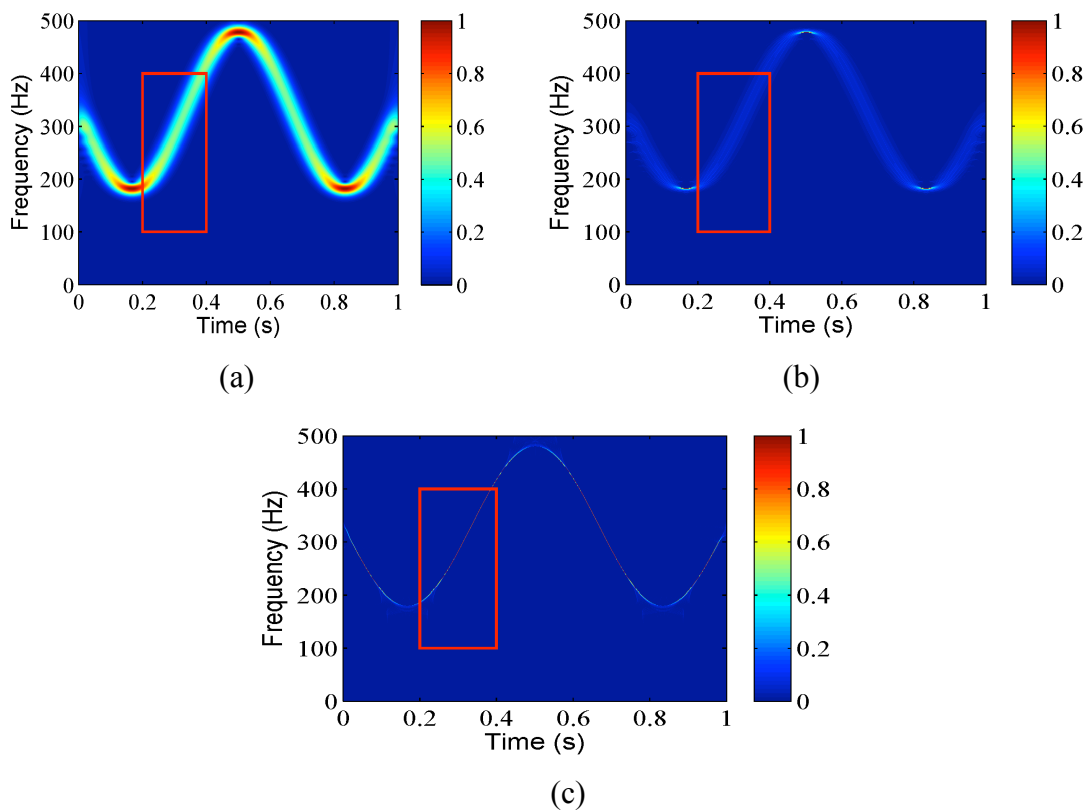| TFA	STFT	FSST	HRSST
Renyi entropy	16.0669	14.5289	10.8801

Fig. 2. Time-frequency maps obtained by STFT (a), FSST (a) and HRSST (c), respectively. HRSST achieves a highly concentrated TFR.
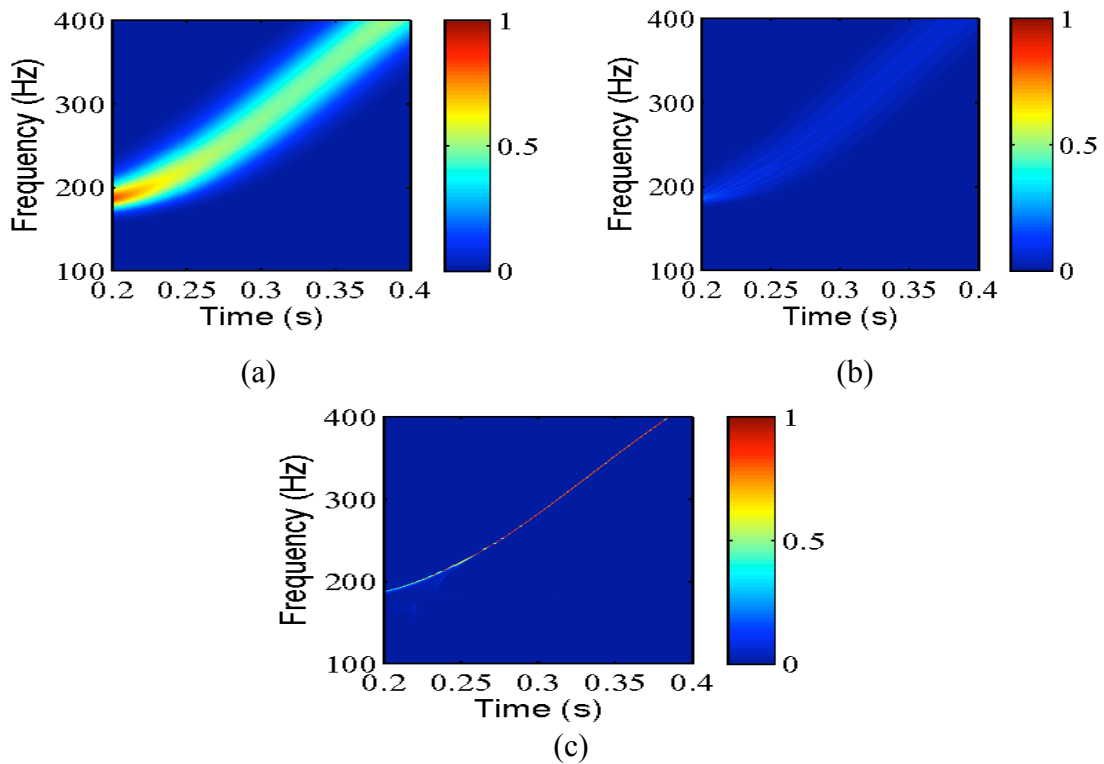

Fig. 3. Local enlarged time-frequency maps corresponding to Fig. 2. The HRSST (b) can generate the more energy-concentrated TFR compared with the STFT (a) and FSST (b) methods.

REAL EXAMPLES

Data Ⅰ

We first apply the STFT, FSST and HRSST methods on a real seismic data (Fig. 4), which is comprised of 150 traces with 500 samples per trace and a sampling interval of 2 ms.   Now, we take the trace 60, shown in Fig. 5(a), as an example to show the TFRs corresponding to the above-mentioned transforms. The result of STFT displays that there are three obvious spectral energies, however, it fails to accurately detect the time of occurrence owing to the poorer time-frequency resolution [Fig. 5(b)]. Both of the FSST and HRSST results exhibit the relatively sparser representation. The difference is that the FSST, squeezing the time-frequency coefficients in the frequency direction, enables the time-frequency energy to spread along the time direction, so that it is difficult to capture the time when the spectral energies appear (Fig. 5(c)). The HRSST makes time-frequency energy concentrated in the time direction. In this sense, it is more beneficial for identifying these existing spectral energies accurately, and thus facilitating further seismic interpretation [Fig. 5(d)].

Next, we extract the 40 and 55 Hz frequency slices after applying the STFT, FSST and HRSST techniques. As reported in Fig. 6, the STFT cannot extract the stratigraphic information effectively due to the influence of time-frequency resolution. The spectral energy from the FSST and HRSST is much sparser than that from the STFT; however, the FSST does not produce a desired result because of the poor time resolution resulting from time-frequency coefficients reassignment in the frequency direction. For the HRSST method, it provides much sparser outputs and depicts the spectral characteristics of seismic reflections more clearly, which is always very important for thin-bed identification.
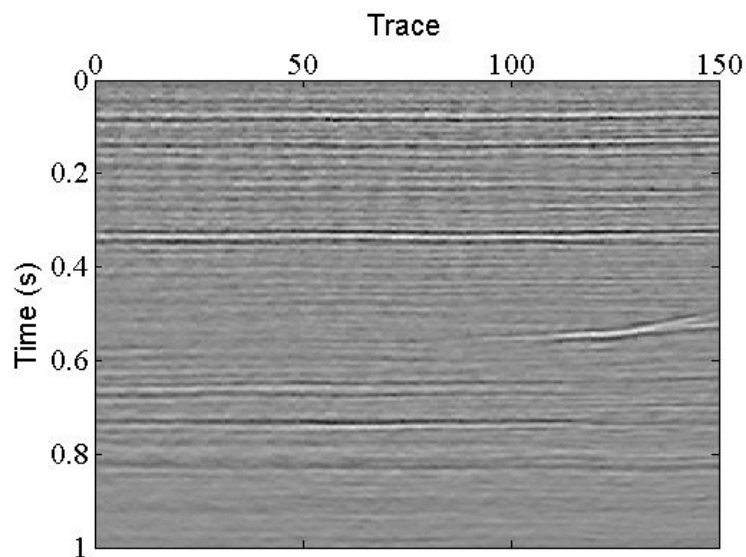

Fig. 4. A field data.
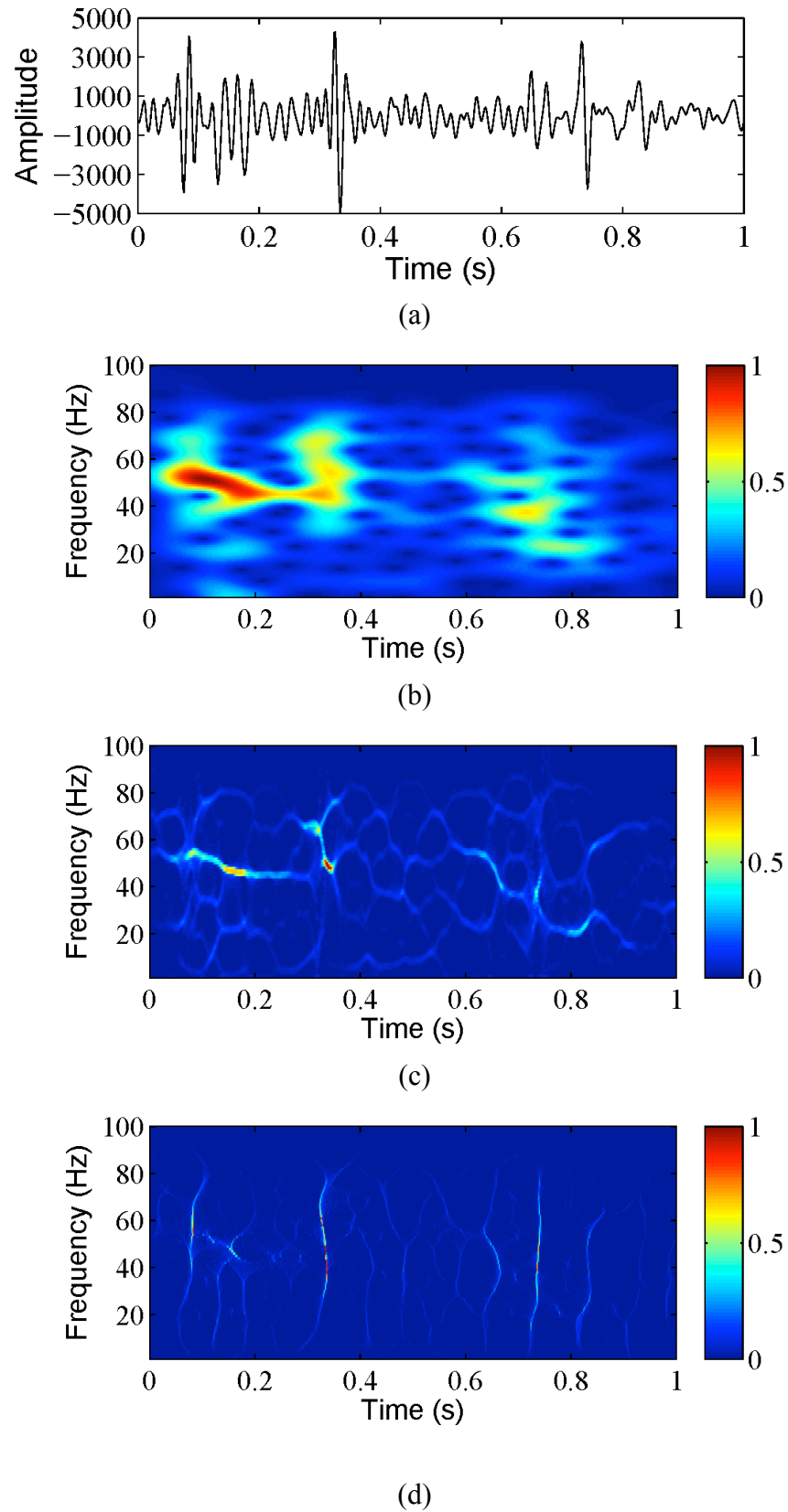
(a)

(b)

(c)

(d)

Fig. 5. Trace 60 from Fig. 7(a), and the corresponding time-frequency maps obtained by STFT (b), FSST (c) and HRSST (d).
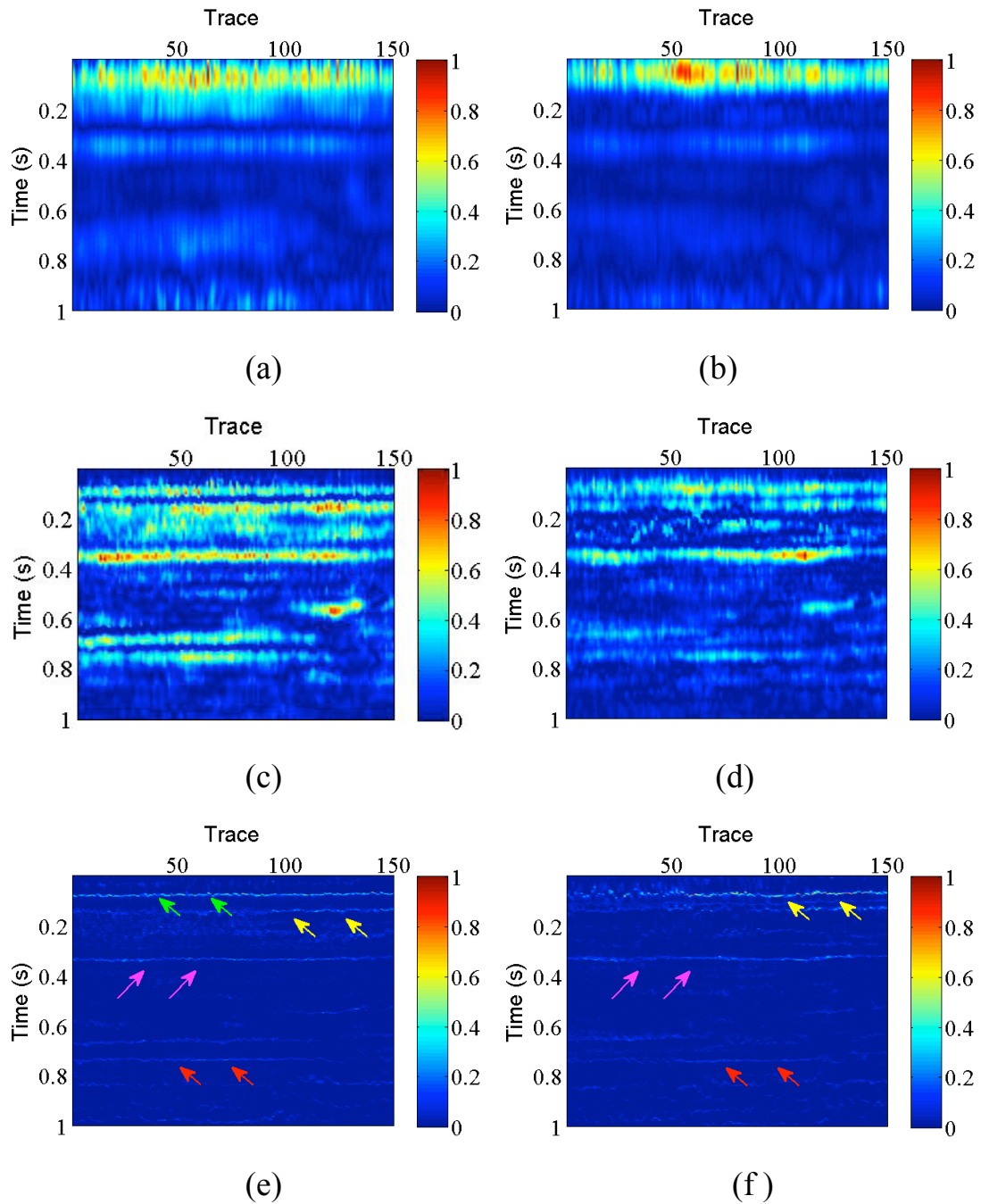
Fig. 6. 40 Hz frequency slices using STFT-based method (a), FSST-based method (c), and HRSST-based method (e). 55Hz frequency slices using STFT-based method (b), FSST-based method (d), and HRSST-based method (f). The HRSST shows the higher time resolution than the STFT and FSST methods.

Data Ⅱ

In this section, a real field data including gas-filled sand is employed to further demonstrate the effectiveness of the HRSST in detection of hydrocarbon. The dataset consists of 60 traces, the record length is 1 s, and the time sampling interval is 2 ms. The gas-filled reservoir is indicated by a

black arrow (Fig. 7) where the seismic trace 20 passes vertically. As shown in Fig. 8(a), there is the obvious strong amplitude around 4s. The TFRs obtained by the STFT, FSST and HRSST are displayed in Figs. 8(b), 8(c) and 8(d), respectively. It can be clearly observed that all TFRs exhibit some similar feature, namely, the strong spectral energy exists at 4s. The FSST and HRSST show more characteristics than the STFT because of the higher time-frequency resolution of both methods. However, the HRSST does a better job accurately describing the instant when the strong spectral energies occur.

Fig. 9 shows the resulting common frequency slices for STFT (a) (b), FSST (c) (d), and HRSST (e) (f) at, respectively, 20 and 40 Hz. A fixed window size makes the STFT show the lower time-frequency resolution. The low-frequency anomaly is more sharply represented by FSST and HRSST than in the STFT maps. The FSST and HRSST have similar performance, that is, the low-frequency anomaly is apparent near the gas-bearing reservoir at 20 Hz, and then the energy is faded at 40Hz. But the HRSST seems to be more able to characterize the exact location of the anomaly owing to higher time resolution, which is helpful to depict the location and extent of the gas-charged sand reservoir further.
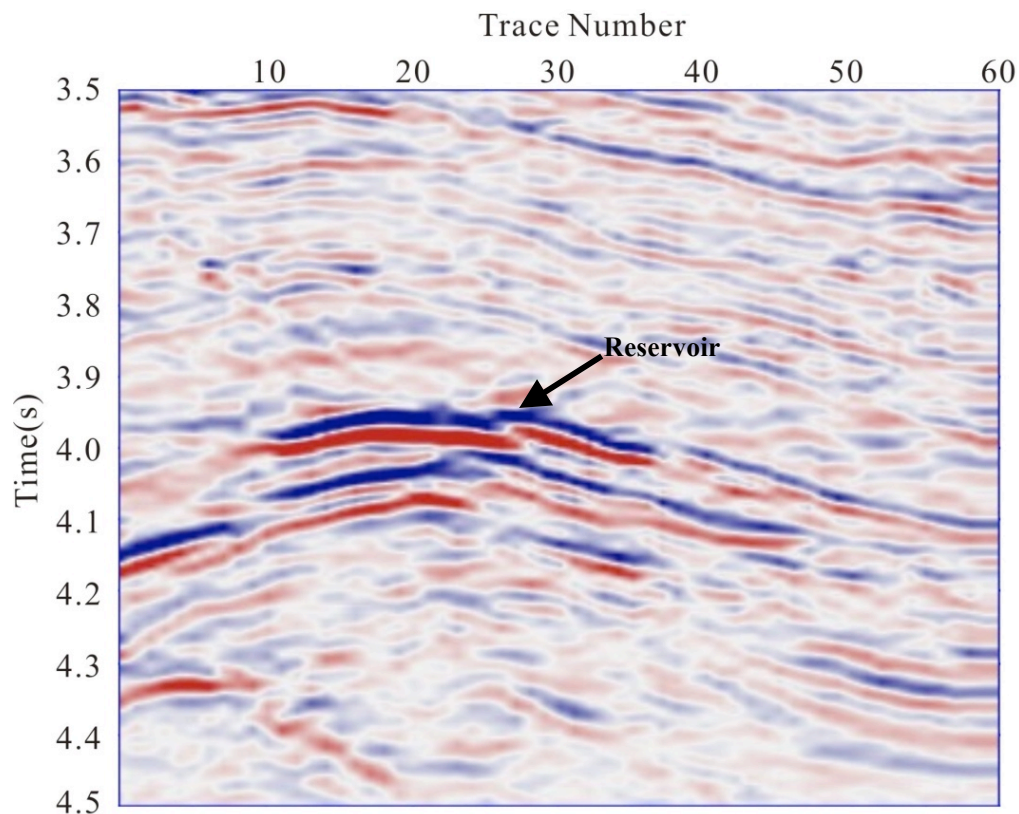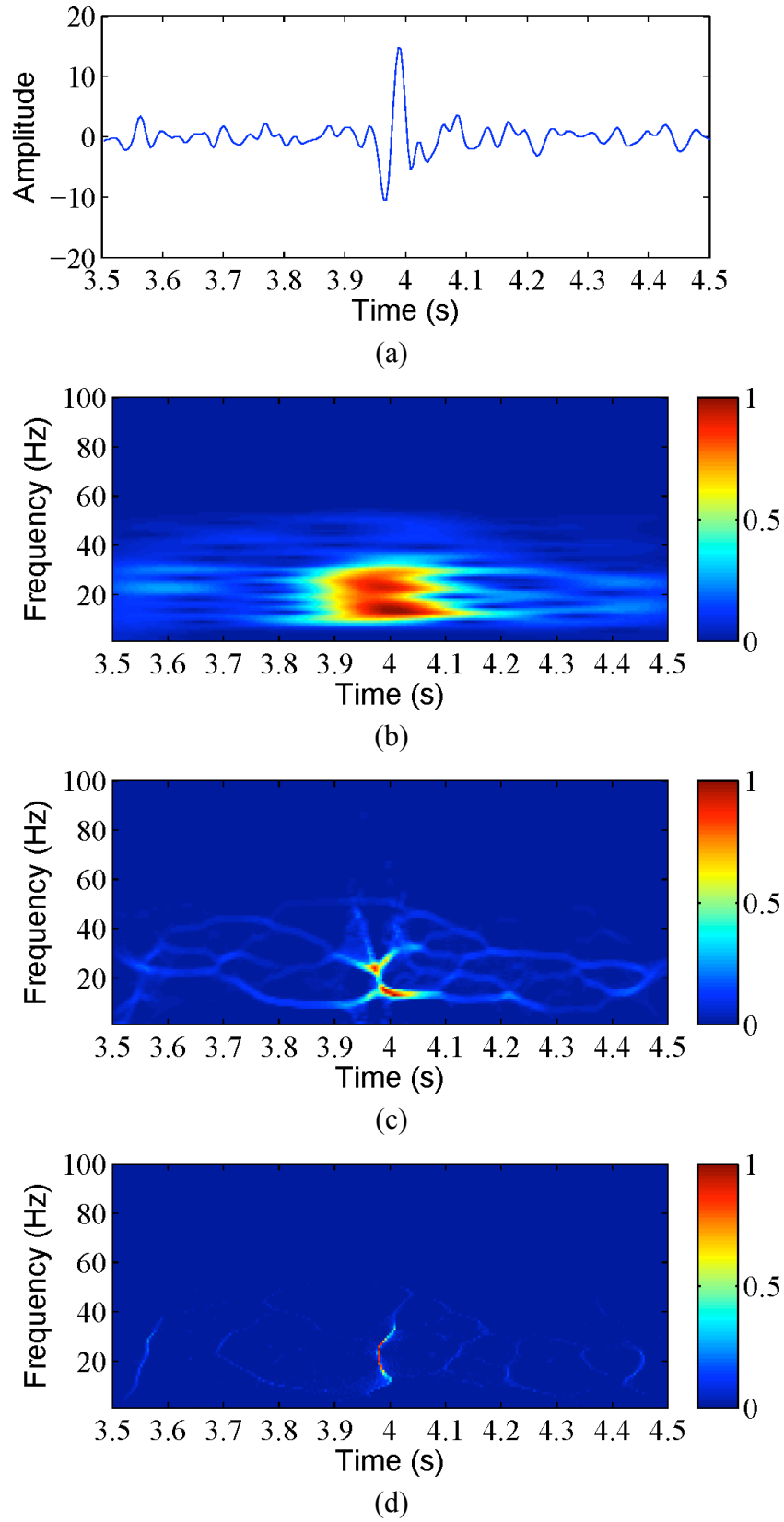

Fig.7. The post-stack data

Fig. 8. Trace 20 from Fig. 7(a), and the corresponding time-frequency maps obtained by STFT (b), FSST (c) and HRSST (d).
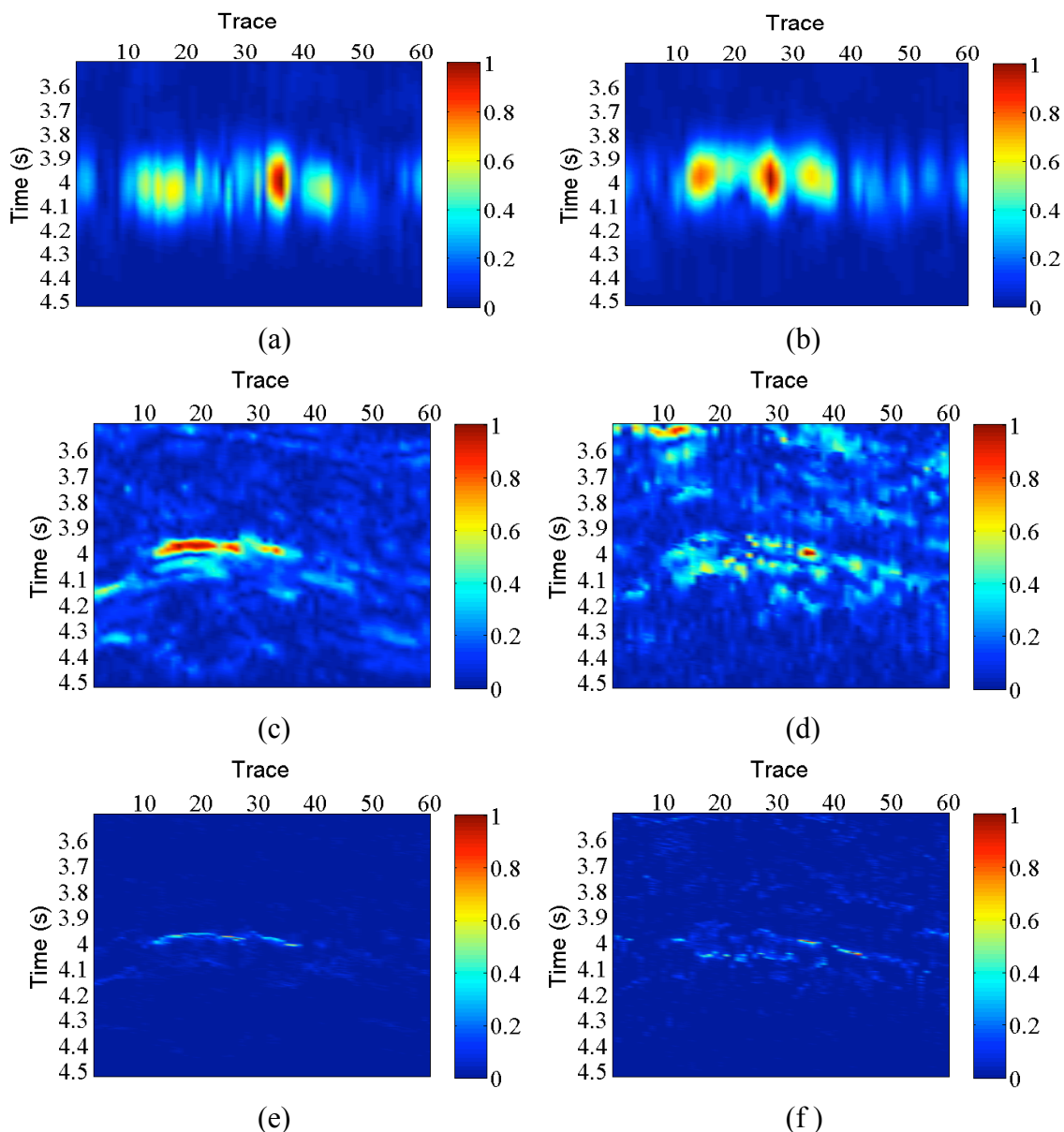
Fig. 9. Constant-frequency slices. (a) (b) The STFT outputs for 20 and 40 Hz, respectively. (c) (d) The corresponding results estimated by FSST. The HRSST outputs are shown in (e) (f). The HRSST shows the higher time resolution than the STFT and FSST methods, and it is beneficial to characterize the exact location of the anomalies.

CONCLUSIONS

In this paper, we proposed a new technique, called HRSST, for seismic time-frequency analysis. The proposed HRSST uses a signal model in the frequency domain, and makes full use of the unbiased group delay estimation to replace the traditional instantaneous frequency calculation, which greatly enhances the time localization. The synthetic data shows that the HRSST achieves a highly energy-concentrated TFR for the signals with a strongly varying instantaneous frequency compared with the STFT and FSST approaches. Field examples further indicate the potential of our method in subsurface geological structures delineation and low-frequency

anomaly detection, which renders that the HRSST is promising for seismic data analysis. Future work will devote to the behavior analysis of the HRSST when applied to noisy signals and the influence of noise on the reassignment operators.

ACKNOWLEDGEMENTS

REFERENCES

Allen, J.B., 1977. Short term spectral analysis, synthetic and modification by discrete Fourier transform. IEEE Transact. Acoust., Speech, Sign. Process., 25: 235-238.

Auger, F. and Flandrin, P., 1995. Improving the readability of time-frequency and time-scale representations by the reassignment method. IEEE Transact. Sign. Process., 43: 1068-1089.

Castagna, J.P., Sun, S. and Siegfried, R.W., 2003. Instantaneous spectral analysis: detection of low-frequency shadows associated with hydrocarbons. The Leading Edge, 22: 120-127.

Chen, Y., Liu, T., Chen, X., Li, J. and Wang, E., 2014. Time-frequency analysis of seismic data using synchrosqueezing wavelet transform. J. Seismic Explor., 23: 303-312.

Daubechies, I., Lu, J. and Wu., H.T., 2011. Synchrosqueezed wavelet transform: An empirical mode decomposition-like tool. Appl. Comput. Harmon. Anal., 30: 243-261.

Daubechies, I. and Maes, S., 1996. A nonlinear squeezing of the continuous wavelet transform based on auditory nerve models. In: Aldroubi, A. and Unser, M. (Eds.), Wavelets in Medicine and Biology. CRC Press, Houston: 527-546.

Herrera, R.H., Han, J. and van der Baan, M., 2014, Applications of the synchrosqueezing transform in seismic time-frequency analysis. Geophysics, 79(3): V55-V64.

Jeffrey, C. and William, J., 1999. On the existence of discrete Wigner distributions. IEEE Sign. Process. Let., 6: 304-306.

Liu, W., Chen W. and Zhang Z. 2020. A novel fault diagnosis approach for rolling bearing based on high-order synchrosqueezing transform. IEEE Access, 8: 12533-12541.

Liu, W. and Chen, W., 2019. Recent advancements in empirical wavelet transform and its applications. IEEE Access, 7: 103770-103780.

Liu, W. and Duan, Z., 2020. Seismic signal denoising using f-x variational mode decomposition. IEEE Geosci. Remote Sens. Lett., 17: 1313-1317.

Liu, Y. and Fomel, S., 2013. Seismic data analysis using local time-frequency decomposition. Geophys. Prospect., 61: 516-525.

Oberlin, T., Meignen, S., and Perrier, V., 2015. Second-order synchrosqueezing transform or invertible reassignment? Towards ideal time-frequency representations. IEEE Transact. Sign. Process., 63: 1335-1344.

Pham, D.H. and Meignen, S., 2017. High-order synchrosqueezing transform for multicomponent signals analysis - With an application to gravitational-wave signal. IEEE Transact. Sign. Process., 65: 3168-3178.

Sinha, S., Routh, P., Anno, P. and Castagna, J., 2005. Spectral decomposition of seismic data with continuous-wavelet transform. Geophysics, 70(6): 19-25.

Thakur, G. and Wu, H.T., 2011. Synchrosqueezing-based recovery of instantaneous frequency from nonuniform samples. SIAM J. Math. Anal., 43: 2078–2095.